Electrochemical properties of surface-confined films of single-walled carbon nanotubes functionalised with cobalt(II)tetra-aminophthalocyanine: Electrocatalysis of sulfhydryl degradation products of V-type nerve agents

Jeseelan Pillay[a] and Kenneth I. Ozoemena[1, a]

[a]Chemistry Department, **University of Pretoria**, Pretoria 0002, South Africa

Abstract

This paper describes detailed comparative electrochemical and electrocatalytic behaviours of basal plane pyrolytic graphite electrodes (BPPGEs) modified with single-wall carbon nanotube (BPPGE-SWCNT) and SWCNTs functionalised with cobalt(II) tetra-aminophthalocyanine by physical (BPPGE-SWCNT-$CoTAPc_{(mix)}$), chemical (BPPGE-SWCNT-$CoTAPc_{(cov)}$) and electrochemical adsorption (BPPGE-SWCNT-$CoTAPc_{(ads)}$) processes. SWCNT improves both solution and surface electrochemistry of CoTAPc. Electrochemical kinetics of the SWCNT-CoTAPc modified BPPGE yielded different k_s values, indicative of different rate-determining steps for the cathodic and anodic reactions. Electrochemical impedance spectroscopy (EIS) analyses in the presence of $[Fe(CN)_6]^{3-/4-}$ as a redox probe revealed that the SWCNT and SWCNT-$CoTAPc_{(mix)}$ films have comparable data in terms of solution resistance (R_s), electron transfer resistance (R_{et}), Warburg impedance (Z_w) and electron-transfer rate constant (k_{app}). Also, these surface-confined films showed comparable electrocatalytic responses towards the detection of V-type nerve agent sulfhydryl hydrolysis products, dimethylaminoethanethiol (DMAET) and diethylaminoethanethiol (DEAET). Using the

BPPGE-SWCNT-CoTAPc$_{(mix)}$, the estimated catalytic rate constants and diffusion coefficients were higher for DEAET than for the DMAET. Also, the detection limits of approximately 8.0 and 3.0 μM for DMAET and DEAET were obtained with sensitivities of 5.0 and 6.0 × 10^{-2} A M^{-1} for DMAET and DEAET, respectively. BPPGE-SWCNT-CoTAPc showed better potential discrimination for detection of these sulfhydryl analytes than the BPPGE-SWCNT, the latter exhibited enhanced catalytic response for the sulfhydryls than the former.

Article Outline

1. Introduction

Carbon nanotubes (CNTs), single-walled (SWCNTs) and multi-walled carbon nanotubes (MWCNTs), have continued to attract intense research interests as ideal nanomaterials for the development of nanoelectronic devices [1], [2] and [3], drug delivery [4], [5] and

[6], and high-performance electrochemical sensors [7], [8], [9], [10] and [11]. These interests are based on the unique properties of CNTs such as high electrical conductivity, high surface area, significant mechanical strength and good chemical stability. SWCNTs have continued to be investigated as viable electrochemical materials because of their unique properties over the less expensive MWCNTs. SWCNTs possess certain special features over the MWCNTs which include smaller size, larger specific area (more than a magnitude [12]), stronger inter-tube attraction and adsorptive properties, and characteristic curve-shaped surface that enables bonding of supramolecular complexes via non-covalent or hydrophobic interactions [13]. Generally, the highly π-conjunctive and hydrophobic sidewalls consisting of sp^2 carbons and open ends bearing oxygen-containing moieties allow them to work as support for organic and inorganic electrocatalysts. This has resulted in the use of CNTs to improve chemical properties of compounds such as porphyrins [14] and amino-containing phthalocyanines [15] and [16] by chemically functionalizing them with CNTs. The π–π interactions of CNT with phthalocyanines in particular stems from the fact that a phthalocyanine molecule is an organic macrocycle with 18 π-electrons.

Cobalt phthalocyanine (CoPc) complexes are well documented as versatile electrocatalysts for a plethora of molecules of industrial, environmental and biomedical relevance [17]. Amino-substituted metallophthalocyanine (MPc) complexes can be covalently linked to CNTs (via amide bond formation [15] and [16]) while unsubstituted MPc complexes are non-covalently adsorbed onto CNTs (via π–π interactions [18]). It is possible that facile co-ordination of these two remarkable π-electron species may well revolutionize their applications as electrocatalysts and in the fabrication of high-performance electrochemical sensors.

Adhesion of CNT onto GCE is difficult and fraught with problems such as irreproducibility [19], therefore the use of basal plane pyrolytic graphite (BPPGE) or edge plane pyrolytic graphite (EPPG) are preferred because of the inherent ability of these electrodes to interact with CNTs via π–π interactions [20], [21] and [22]. As part of our on-going investigations geared towards harnessing the twin properties of electroactive amino-substituted transition MPc (notably, the CoTAPc) complexes and CNTs [23] and [24], this work is aimed at investigating the electrochemical and

electrocatalytic features of BPPGE modified with SWCNT-CoTAPc prepared by chemical (covalent) attachment and simple physical (ultrasonication) means. For better comparative insights, three different types of BPPGE-SWCNT-CoTAPc were fabricated: (i) CoTAPc electrochemically adsorbed onto a BPPGE pre-modified with SWCNT (herein referred to as BPPGE-SWCNT-CoTAPc$_{(ads)}$), (ii) covalently linked SWCNT-CoTAPc immobilised onto a BPPGE (i.e., BPPGE-SWCNT-CoTAPc$_{(cov)}$) and (iii) a composite form or mixture of SWCNT and CoTAPc immobilised onto a BPPGE (i.e., BPPGE-SWCNT-CoTAPc$_{(mix)}$). Electrochemical techniques have been well established to provide excellent insights into the adsorption and reactivity of surface-modified redox-active species. Thus, in this work, we interrogated the redox-activity SWCNT-CoTAPc modified BPPGEs using cyclic voltammetry and electrochemical impedance spectroscopy (EIS) with $[Fe(CN)_6]^{3-/4-}$ system as a redox probe.

The serious threats posed to the society by terrorists have made the fast detection of organophosphates based chemical warfare agents (CWAs), especially those of the V-type nerve agents and their sulfhydryl hydrolysis products [25] and [26] (Table 1) a major global concern. Thus, in this work, we investigated the possible applications of the modified BPPGEs as viable devices for the study of the electrocatalysis and sensing of sulfhydryl degradation products of CWAs, i.e., those of the V-type nerve agents, diethylaminoethanethiol (DEAET) and dimethylaminoethanethiol (DMAET) (Table 1) in aqueous solution.

Table 1.

Molecular structures of “V”-type nerve agents and their corresponding hydrolysis products

CWAs (V-type nerve agents)	**Actual hydrolysis product**	**Hydrolysis product mimics studied in this work**
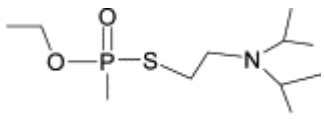 **VX**	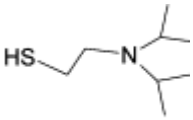 **DIPAET**	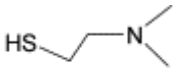 **DMAET**
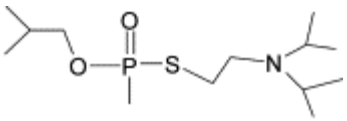 **R-VX**	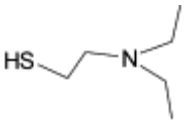 **DEAET**	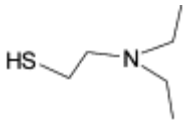 **DEAET**

Nerve agents have been described as the poor man's atomic bomb and are being used by terrorists to develop chemical weapons. Upon chemical or enzymatic hydrolysis, the V-type nerve agents, VX [*O*-ethyl-*S*-(2-diisopropylaminoethyl)methylphosphonothioate] and its Russian analogue R-VX [*O*-isobutyl-*S*-(2-diethylaminoethyl)methylphosphonothioate] generate sulfhydryl moieties such as the diisopropylaminoethanethiol (DIPAET), DMAET and DEAET [25] and [26]. These sulfhydryl degradation products are far more stable in the environment than their parent V-type nerve agents, meaning that they can be easily utilised to provide a reliable indication of the parent nerve agents. To our knowledge, this study provides the first detailed attempt undertaken to prove the redox-activity of SWCNT co-ordinated with any MPc complex. It also represents the first electrocatalytic studies of thiol hydrolysis products of nerve agents.

2. Experimental

2.1. Materials and reagents

Single-walled carbon nanotube was purchased from Aldrich. Cobalt tetra-aminophthalocyanine (CoTAPc) complex was synthesized and characterized according to established procedures [27], [28] and [29]. Basal plane pyrolytic graphite (BPPGE) plate from which the BPPGE was fabricated was obtained from Le Carbone (Sussex, UK). The Norton carborundum paper (p1200C) used to clean the electrode was purchased from Saint-Gobain Abrasives (Saint-Gobain Abrasives (pty) Ltd., Isando, South Africa). 2-(Dimethylamino)ethanethiol (DMAET) and 2-(diethylamino)ethanethiol (DEAET) were obtained from Sigma. *N*,*N*-Dimethylformamide (DMF) was obtained from Sigma–Aldrich. Tetrabutylammonium tetrafluoroborate ($TBABF_4$), used as electrolyte, was obtained from Aldrich. Pyridine from obtained from SAARCHEM (South Africa). Ultra pure water of resistivity 18.2 MΩ was obtained from a Milli-Q Water System (Millipore Corp., Bedford, MA, USA) and was used throughout for the preparation of solutions. Phosphate buffer solutions (PBS) at various pHs were prepared with appropriate amounts of KH_2PO_4 and K_2HPO_4, and the pH adjusted with 0.1 M H_3PO_4 or NaOH. All electrochemical experiments were performed with nitrogen-saturated phosphate buffer, except for the potassium ferricyanide solutions, which were prepared in 0.05 M

potassium chloride (all solutions nitrogen saturated as well). All other reagents were of analytical grade and were used as received from the suppliers without further purification. Briefly, the starting material SWCNT (Aldrich) was first purified and cut into short and uncapped nanotubes bearing acidic functions (SWCNT-COOH) according to the multi-step procedures developed by Smalley and co-workers [30] by refluxing in 2.6 M HNO_3, ultrasonicaton in a mixture of concentrated H_2SO_4 and HNO_3 (3:1, v/v) and suspension in a mixture of concentrated H_2SO_4 and 30% aqueous H_2O_2 (4:1, v/v). IR[(KBr) V_{max} (cm^{-1})]: 3461 (O–H), 2922, 1616 (C═O). The obtained SWCNT-COOH were converted to acyl chlorides moieties (SWCNT-COCl) by reaction with excess thionyl chloride ($SOCl_2$) containing catalytic amount of DMF at 70 °C for 72 h, following the procedure described by Haddon and co-workers [31]. Preparation of the CoTAPc-SWCNT systems via amide-bond formation were carried out using (a) the established multi-step chemical procedures [15] and [16] involving the reaction of SWCNT-COCl and CoTAPc (herein abbreviated as CoTAPc-$SWCNT_{(cov)}$), and (b) simple ultrasonication of a mixture of SWCNT-COOH and CoTAPc (herein abbreviated as CoTAPc-$SWCNT_{(mix)}$) (Scheme 1).

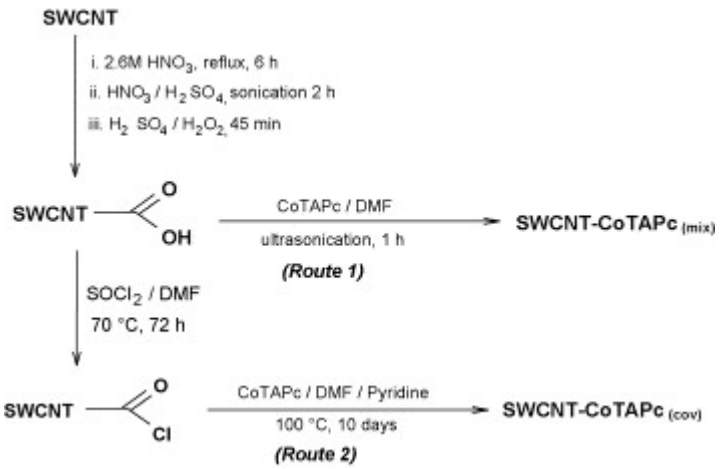

Scheme 1. Schematic representation of the preparation of carboylated single-walled carbon nanotube (SWCNT-COOH) by acid-treatments and subsequent functionalization with cobalt(II)tetra-aminophthalocyanine (SWCNT-CoTAPc) by physical (route 1) and chemical (route 2) methods.

A composite form of the SWCNT-CoTAPc system was obtained by simple ultrasonication (route 1) of a mixture of CoTAPc and SWCNT-COOH (1:1, w/w) in DMF at 1000 rpm for 1 h. The solution was then decanted, centrifuged, and vacuum-dried. The product is herein abbreviated as SWCNT-CoTAPc$_{(mix)}$. IR[(KBr) V_{max} (cm^{-1})]: 3420 (O–H, N–H), 1562 (C═O). Covalent coordination of the CoTAPc with SWCNT via amide-bond formation (route 2) was carried out using the established multi-step chemical procedures [15] and [16] involving the reaction of SWCNT-COCl and CoTAPc (herein abbreviated as CoTAPc-SWCNT$_{(cov)}$). Briefly, SWCNT-COCl (25 mg) was reacted with 0.15 g of CoTAPc in 25 ml of DMF mixed with several drops of pyridine at 100 °C for 10 days. Excess CoTAPc was removed completely by washing with dry DMF giving a black solid product (SWCNT-CoTAPc$_{(cov)}$) (~0.4 mg) after centrifugation, thorough cleaning and vacuum-drying. IR[(KBr) V_{max} (cm^{-1})]: 3377 (N–H), 1576 (C═O).

2.2. Apparatus and procedure

All electrochemical experiments were carried out using an Autolab Potentiostat PGSTAT 30 (Eco Chemie, Utrecht, The Netherlands) driven by the General Purpose Electrochemical Systems data processing software (GPES, software version 4.9). Square wave parameters were: step potential 5 mV; equilibration time 5 s; amplitude 25 mV at a frequency of 15 Hz. Electrochemical impedance spectroscopy (EIS) measurements were performed with an Autolab FRA software between 1.0 Hz and 10 kHz using a 5 mV rms sinusoidal modulation in a solution of 1 mM of $K_4Fe(CN)_6$ and 1 mM $K_3Fe(CN)_6$ (1:1) mixture containing 0.1 M KCl, and at the $E_{1/2}$ of the $[Fe(CN)_6]^{3-/4-}$ (0.124 V versus Ag|AgCl). A non-linear least squares (NNLS) method based on the EQUIVCRT programme developed by Boukamp [32] was used for fitting the obtained EIS data. TEM was performed with Multi-purpose TEM (Philips 301). Energy-dispersive X-ray (EDX) was performed with JEOL 840 at 5 kV accelerating voltage. A conventional three-electrode system was used. BPPGE disk (d = 5 mm in Teflon) used as working electrode was fabricated in-house. Electrical contact with the disk was obtained via an inserted copper wire held in place with conducting silver varnish L 100 (Kemo® Electronic, Germany). The working electrode was plane BPPGE disk or BPPGE modified with

SWCNTs (BPPGE-SWCNT) or BPPGE modified with SWCNTs and cobalt tetra-aminophthalocyanine by electrodeposition (designated as BPPGE-SWCNT-CoTAPc$_{(ads)}$). In some cases, the BPPGE electrode modified directly with CoTAPc by electropolymerization, was employed as a working electrode. A Ag|AgCl wire and platinum wire were used as pseudo-reference and counter electrodes, respectively. A Wissenschaftlick-Technische Werkstätten (WTW) pH 330/set-1 (Germany) pH meter was used for pH measurements. All solutions were de-aerated by bubbling nitrogen prior to each electrochemical experiment. All experiments were performed at 25 ± 1 °C.

2.2.1. Electrode modification and pretreatments

The in-house fabricated BPPGE surface was first cleaned as reported before [23] and [24] by gentle polishing on a carborundum paper, followed by cleaning with cellotape-process of removing graphite layers and finally rinsing in acetone to remove any adhesive. The modified BPPGEs (BPPGE-SWCNT, BPPGE-SWCNT-COOH, BPPGE-CoTAPc, BPPGE-SWCNT-COTAPc$_{(cov)}$ and BPPGE-SWCNT-COTAPc$_{(mix)}$) were obtained by placing a drop of the DMF solution of the required modifier onto the BPPGE surface and drying in an oven at 80 °C. The BPPGE-SWCNT-CoTAPc$_{(ads)}$ was obtained as described before [24] by electrosorption process, which involves repetitive cyclic voltammetric scanning (50 scans) of a BPPGE-SWCNT-COOH in a DMF solution of 10^{-3} M CoTAPc containing $TBABF_4$ (10^{-2} M). CoTAPc exhibits poor solubility in DMF, thus the CoTAPc-DMF solution was left for about 4 days for in an air-tight container to allow for the complete dissolution of the CoTAPc before electrodeposition process. Also, the modified electrodes were conditioned for electrocatalytic studies by repetitive cycling in 0.1 M phosphate buffer solutions of either pH 4.0 or pH 7.0 until a stable cyclic votammogram was obtained.

3. Results and discussion

3.1. Characterization of SWCNT-CoTAPc

Unlike the pristine SWCNT, the SWCNT-COOH exhibited good solubility in DMF with no detectable precipitate even after 6 months. Also, while CoTAPc easily forms precipitate in DMF, the SWCNT-CoTAPc systems, especially the SWCNT-CoTAPc$_{(cov)}$,

did not form any detectable precipitate even after 6 months, thus suggesting an enhanced solubility of CoTAPc in organic solvents due to the coordination with SWCNT-COOH. Similar results have been reported for MWCNT-MnTAPc [18]. The IR spectral data of both the SWCNT-CoTAPc$_{(cov)}$ and SWCNT-CoTAPc$_{(mix)}$ showed the C═O stretching from the –CONH– group in the 1562 and 1576 region, indicative of covalent interaction between the –COOH of the acid-treated SWCNT and the –NH_2 of the CoTAPc complex. As expected, the TEM images (not shown) confirmed the conversion of the pristine SWCNT to short nanotubes. The acid-treated SWCNT was seen entangled with the CoTAPc, indicative of the strong interactions between these two π-electron species. SWCNT-CoTAPc$_{(mix)}$ and SWCNT-CoTAPc$_{(cov)}$ were found to be more soluble than CoTAPc in organic solvents, consistent with the previous observation for MnTAPc-MWCNT [18]. Fig. 1 shows typical square wave voltammograms (SWV) of solution electrochemistry of both CoTAPc (a) and SWCNT-CoTAPc$_{(mix)}$ (b). Both complexes did not show significant difference in terms of potentials. However, due to the enhanced solubility, CoTAPc-SWCNT species showed well-resolved voltammograms compared to the CoTAPc. From the well-documented electrochemistry of CoPc complexes [33], the redox processes IV (−0.31 V) and V (0.80 V for CoTAPc-SWCNT and 0.90 V for CoTAPc) are due to the central cobalt redox processes Co^{II}/Co^{I} and Co^{III}/Co^{II}, respectively, while other peaks I, II, III and VI are due to phthalocyanine ring processes. The enhancement of the Co^{III}/Co^{II} process is an indication that the SWCNT markedly promote the electron-transfer reaction of the CoTAPc in this solvent system.

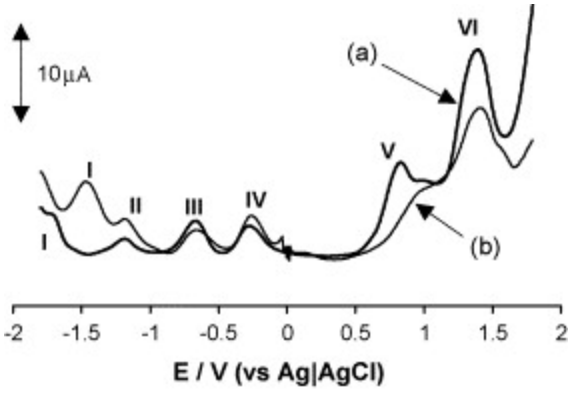

Fig. 1. Square wave voltammograms of (a) CoTAPc-SWCNT$_{(mix)}$ and (b) CoTAPc in DMF containing $TBABF_4$.

3.2. Electrochemistry of modified BPPGEs

Fig. 2 presents typical cyclic voltammetric responses obtained during 50 repetitive scans of BPPGE-SWCNT in DMF solutions of CoTAPc containing $TBABF_4$. Both cathodic and anodic voltammetric waves decreased continuously from the first scan and then remained stable until about the 30th scans when redox peaks finally disappeared.

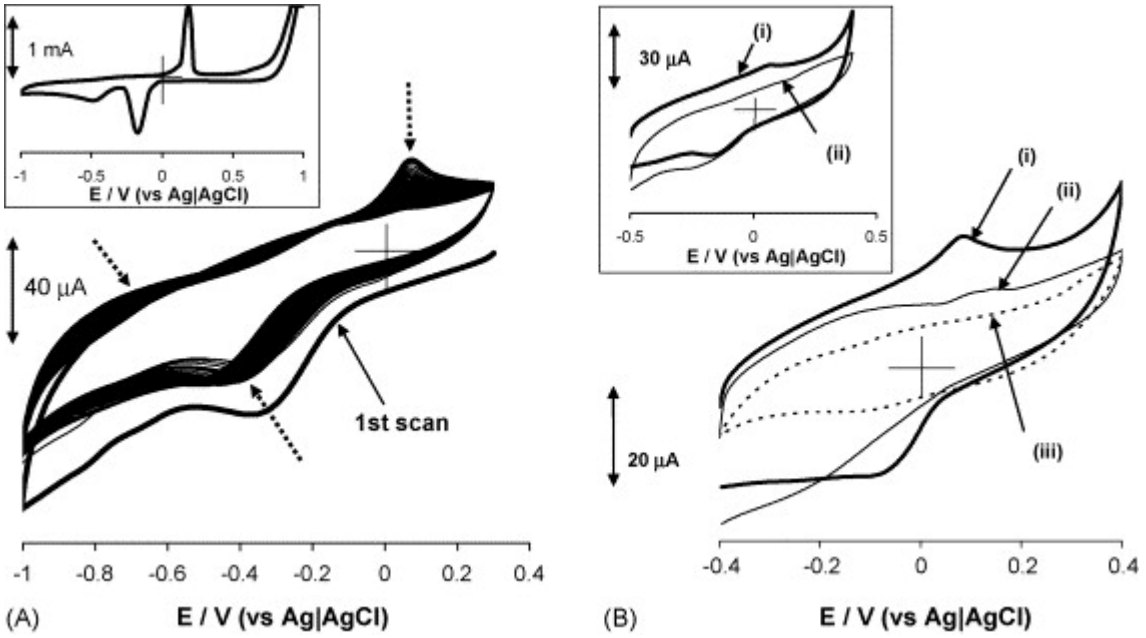

Fig. 2. (A) Cyclic voltammetric profiles for electrosorption process (50 scans) of a 1 mM CoTAPc in DMF containing $TBABF_4$ at a BPPGE-SWCNT. Inset depicts the final (20th scan) scan obtained during conditioning of BPPGE-SWCNT-$CoTAPc_{(ads)}$ in pH 4.4 PBS. (B) Comparative CVs of (i) BPPGE-SWCNT-$CoTAPc_{(ads)}$, (ii) BPPGE-SWCNT and (iii) bare BPPGE in PBS (pH 4.4). Inset represents (i) BPPGE-SWCNT-$CoTAPc_{(ads)}$ and (ii) BPPGE-SWCNT in pH 7.4. Scan rate, 50 mV s^{-1}.

As stated in a previous report [24], this behaviour is indicative of electrosorption process [34], [35] and [36], which suggests π–π interaction between the benzene rings of the phthalocyanine and the sidewalls of the immobilised SWCNT at the BPPGE. We also observed electropolymerization process (i.e., growth in anodic and cathodic peaks during our experiments) (not shown) but only when CoTAPc was still dissolving in DMF. Thus, all electrochemical deposition experiments for CoTAPc were carried out only when the CoTAPc was completely solubilized in the DMF, in which case only electrosorption was

observed. Fig. 2A inset exemplifies typical CVs obtained after conditioning of the electrodes obtained via electrosorption in pH 4.4 PBS. Electrochemical conditioning for the electrode obtained via electrosorption resulted in the formation of a well-defined reversible couple of anodic-to-cathodic peak currents (I_{pa}/I_{pc}) of one, peak–peak separation ($\Delta E_p = E_{pa} - E_{pc}$) of approximately 0.34 V (versus Ag|AgCl)) and half-wave potential ($E_{1/2} = (E_{pa} + E_{pa})/2$) of 0.05 V. We attribute this reversible electrochemistry to re-arrangement of the electrosorbed redox-active CoTAPc film on the BPPGE-confined redox-active SWCNT. This observation is rare and needs further investigations. At this moment, however, we may explain this reorganisation process as follows: during the electrosorption of the CoTAPc onto the immobilised SWCNT, it is reasonable to presume that there is inclusion or trapping or inter-linking of the solvent/electrolyte molecules between the SWCNT and CoTAPc leading to a 'wide' SWCNT|CoTAPc interface. The continuous voltammetric cycling (electrochemical pre-treatment) of the electrosorbed CoTAPc film in aqueous solution leads to the exclusion of these inter-linked solvent/electrolyte molecules, narrowing the gap of the SWCNT|CoTAPc interface, thereby allowing much closer contact of the CoTAPc with the SWCNT. Each voltammetric cycling results in partial destruction of the inter-linkage and brings the CoTAPc ring closer to the underlying SWCNT, hence the subsequent increase in the redox wave (at the ~0.05 V versus Ag|AgCl) of the SWCNT-CoTAPc at every scan. At about the 20th scan, the CV remained stable and started to decrease [24], signifying the end of this reorganisation of the initial SWCNT|CoTAPc interface. The decrease in the current response after stabilisation is certainly due to the loss of the weakly attached CoTAPc species. We have no firm explanation to the preferential electrosorption of CoTAPc at our experimental conditions but could possibly be due to the special features of the SWCNTs such as their large specific area as well as strong inter-tube attraction and adsorptive properties [12].

Fig. 2B compares the cyclic voltammograms obtained in PBS pH 4.4 for the conditioned BPPGE-SWCNT-CoTAPc$_{(ads)}$ (i), BPPGE-SWCNT (ii) and the bare (iii). The $E_{1/2}$ of the electrosorbed CoTAPc is approximately zero volt while its peak–peak separation (ΔE) is ~0.2 V (versus Ag|AgCl) when compared to similar CV experiments in pH 7.4 (Fig. 2B inset) of $E_{1/2}$ of approximately −0.10 V and ΔE ~ 0.30 V (versus Ag|AgCl), indicating

weak electron transfer process in pH 7.4. It should be mentioned that SWCNT sometimes shows intrinsic redox processes in aqueous solution as a result of the oxygen-containing moieties (e.g., carboxyl, hydroxyl, and quinone-like groups) on the defects and opened caps of the SWCNT [36] and [37]. These intrinsic redox processes may well explain the broad voltammograms observed for the BPPGE-SWCNT, for example the weak anodic peak in the ~0.1 V region in pH 4.4 (Fig. 2B(ii)). Similar CV evolution for the BPPGE-SWCNT-CoTAPc$_{(ads)}$ in the buffered aqueous solutions were also obtained for the BPPGE-SWCNT-CoTAPc$_{(mix)}$ and BPPGE-SWCNT-CoTAPc$_{(cov)}$ obtained by drop-dry process. It is reasonable therefore to associate the single redox couple obtained for the BPPGE-SWCNT-CoTAPc$_{(ads)}$ (i), especially the broad cathodic peak, to be the consequence of the overlapped redox processes of the SWCNT, the phthalocyanine ring as well as the irreversible Co^{II}/Co^{I}. The surface coverage (Γ_{MPc} (mol cm^{-2})) of each of the three CoTAPc-based electrodes was estimated from this well-defined redox couple in pH 4.4 solutions from the background-corrected charge, Q, under the anodic peaks at 50 mV s^{-1} using the following relationship [38]:

$$\Gamma_{MPc} = \frac{Q}{nFA} \quad (1)$$

where n represents number of electrons transferred (assume ≈1), F the Faraday constant (96,485 C mol^{-1}), and A is the geometric surface area of the electrode (~0.192 cm^2). The surface coverage was found to be *ca*. 1.0×10^{-9} mol cm^{-2}.

As expected for surface-confined redox species, the response of the single redox couple of the BPPGE-SWCNT-CoTAPc$_{(mix)}$, BPPGE-SWCNT-CoTAPc$_{(cov)}$ and BPPGE-SWCNT-CoTAPc$_{(ads)}$ (at $E_{1/2} \approx 0.0$ V and $\Delta E \approx 0.2$ V versus Ag|AgCl) with changing scan rates (25–1500 mV s^{-1}) resulted in a linear increase of the redox currents with scan rates at low scan rates. At scan rates >100 mV s^{-1}, however, the cathodic waves became severely distorted. This type of distortion is an indication that the electrode reaction becomes electrochemically irreversible at higher scan rates. Such irreversible electrode reaction follows the Laviron's theory [39] and [40]:

$$E_{pc} = E^{o'} + \frac{RT}{\alpha n F} \ln \frac{RTk_s}{\alpha n F} - \frac{RT}{\alpha n F} \ln v \quad (2)$$

$$E_{pa} = E^{o'} + \frac{RT}{(1-\alpha) n F} \ln \frac{RTk_s}{(1-\alpha) n F} - \frac{RT}{(1-\alpha) n F} \ln v \quad (3)$$

where $E^{o'}$ (or $E_{1/2}$) is the formal potential, □ the electron transfer coefficient, k_s the standard rate constant of the surface reaction, and v is the scan rate. As identified in Fig. 2, electrochemical reversibility was better at pH 4.4 solution than at ≥pH 7.4, thus this electrochemical kinetic study was carried out in the pH 4.4 solutions for the BPPGE-SWCNT-CoTAPc$_{(mix)}$ and BPPGE-SWCNT-CoTAPc$_{(cov)}$ obtained by drop-dry method. At high scan rates, the plots of E_p versus ln v (and $E^0 \approx 0$ V versus Ag|AgCl) were linear. The equation of the straight lines were:

• For the BPPGE-SWCNT-CoTAPc$_{(mix)}$:

$$E_{pa}=0.1312 \ln v+0.3712 \ (r^2=0.9969) \quad (4)$$

$$E_{pc}=-0.1970 \ln v-0.7171 \ (r^2=0.9975) \quad (5)$$

• For the BPPGE-SWCNT-CoTAPc$_{(cov)}$:

$$E_{pa}=0.0987 \ln v+0.3497 \ (r^2=0.9867) \quad (6)$$

$$E_{pc}=-0.1883 \ln v-0.6995 \ (r^2=0.9854) \quad (7)$$

For the BPPGE-SWCNT-CoTAPc$_{(mix)}$, the cathodic parameters □n and k_s, were estimated as 0.13 and 0.13 s^{-1}, respectively, while those of the anodic process $(1 - \alpha)n$ and $k_s$were approximately 0.20 and 129 s^{-1}, respectively. Also for the BPPGE-SWCNT-CoTAPc$_{(cov)}$, the □n and k_s, were estimated as 0.14 and 0.13 s^{-1}, respectively, while $(1 - \alpha)n$ and k_s were approximately 0.26 and 350 s^{-1}, respectively. These values are in the similar range as previously reported for the BPPGE-SWCNT-CoTAPc$_{(ads)}$ [24]. These data clearly suggest that the rate-determining steps of the cathodic and anodic reactions are different. We attribute the smaller k_s values for the cathodic reactions as the result of weak electron transfer process arising from the complications of the overlapped reactions

as already described above. As seen in our previous works [41], this behaviour of one redox wave exhibiting higher peak current than its reverse wave is typical of CoPc and its complexes.

3.2.1. Electrochemical impedance spectroscopic investigations

Electrochemical impedance spectroscopy (EIS) measurements were used to investigate the complex electrochemical behaviour of the modified BPPGEs. EIS serves an effective technique for interrogating the kinetics at interfaces and to distinguish between the various mechanisms that govern charge transfer [42] and [43]. Prior to EIS experiments, the CVs of the $[Fe(CN)_6]^{3-/4-}$ redox probe in 0.1 M KCl were run using the different electrodes. Such CV experiments serve as initial insights into the electron transfer processes at the modified electrodes. Fig. 3 presents typical modified BPPGEs; (i) BPPGE-SWCNT-CoTAPc$_{(cov)}$, (ii) BPPGE-CoTAPc, (iii) BPPGE-SWCNT-CoTAPc$_{(mix)}$, (iv) BPPGE-SWCNT and (v) bare BPPGE. Unlike the bare BPPGE, the modified BPPGEs gave well-defined redox peaks for the redox probe. The BPPGE modifiers act as redox mediators by enhancing the electronic communication between the BPPGE and the $[Fe(CN)_6]^{4-}/[Fe(CN)_6]^{3-}$ species. The ΔE_p were estimated as 105, 105, 102, and 128 mV (versus Ag|AgCl) for the BPPGE-CoTAPc, BPPGE-SWCNT, BPPGE-SWCNT-CoTAPc$_{(mix)}$ and BPPGE-SWCNT-CoTAPc$_{(cov)}$, respectively. This results indicates a relatively faster electron transfer process at the BPPGE-SWCNT-CoTAPc$_{(mix)}$ compared to other electrodes.

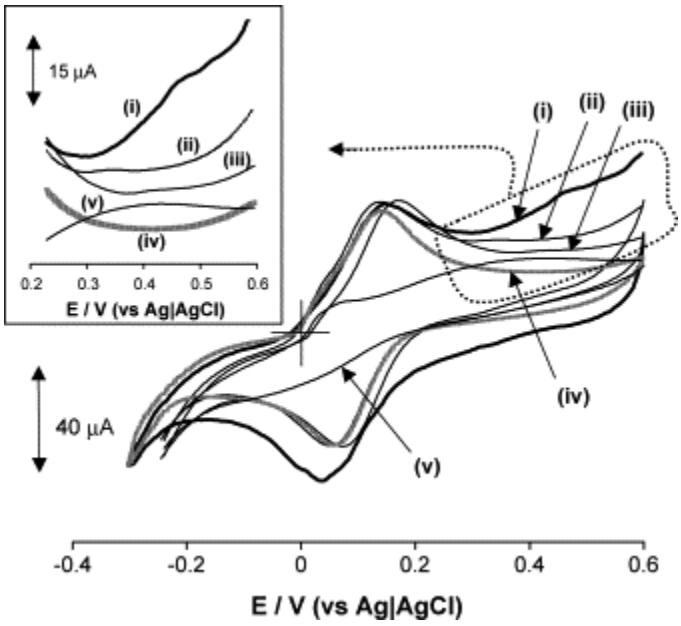

Fig. 3. CV profiles of $[Fe(CN)_6]^{3-/4-}$ resulting from (i) BPPGE-SWCNT-CoTAPc$_{(cov)}$, (ii) BPPGE-CoTAPc, (iii) BPPGE-SWCNT-CoTAPc$_{(mix)}$, (iv) BPPGE-SWCNT and (v) bare BPPGE in 0.1 M KCl containing equimolar mixture of $K_4Fe(CN)_6$ and $K_3Fe(CN)_6$. Scan rate, 25 mV s^{-1}. Expanded portion (inset) is meant to show the Co^{II}/Co^{III} redox couple of the CoTAPc-based electrodes.

The successful attachment of the CoTAPc film onto SWCNT is evident from the Co^{III}/Co^{II} redox couples (expanded in Fig. 3 inset for clarity). The E_p for Co^{III}/Co^{II} are *ca.* 0.35, 0.43, 0.46 and 0.36 V (versus Ag|AgCl) for BPPGE-CoTAPc, BPPGE-SWCNT-CoTAPc$_{(mix)}$, BPPGE-SWCNT-CoTAPc$_{(cov)}$ and BPPGE-SWCNT-CoTAPc$_{(ads)}$, respectively. These Co^{III}/Co^{II} couples are irreversible. Irreversibility of the Co^{III}/Co^{II} process is characteristic of adsorbed CoPc complexes [44]. The high value for SWCNT-CoTAPc compared to CoTAPc is consistent with introduction of electron-withdrawing substituents to MPc ring. Introduction of electron-withdrawing substituents to MPc ring lead to a decrease on the average electron density on the total conjugated Pc system leading to difficult oxidation.

For further insights into the electron transfer at the modified BPPGEs, EIS experiments were carried out in the same conditions as for Fig. 3 with potential fixed at $E_{1/2}$ = 0.13 V versus Ag|AgCl, which is the formal of $[Fe(CN)_6]^{3-/4-}$ obtained in Fig. 3. The Nyquist plots ($Z_{imaginary}$ versus Z_{real}) (Fig. 4A(i–vi)) exhibited the characteristics semicircles at

high frequencies and a straight line at low frequencies, corresponding to kinetic and diffusion processes, respectively. Thus, to fit the EIS data, we modelled the spectra following the simple equivalent circuit of mixed kinetic and diffusion control shown in Fig. 4B, where R_s is the resistance of the electrolyte and electrode contacts, R_{et} is the charge-transfer resistance (domain of kinetic control) and Z_w is the Warburg impedance (domain of mass transport control) resulting from the diffusion of ions to the electrode interface from the bulk of the electrolyte.

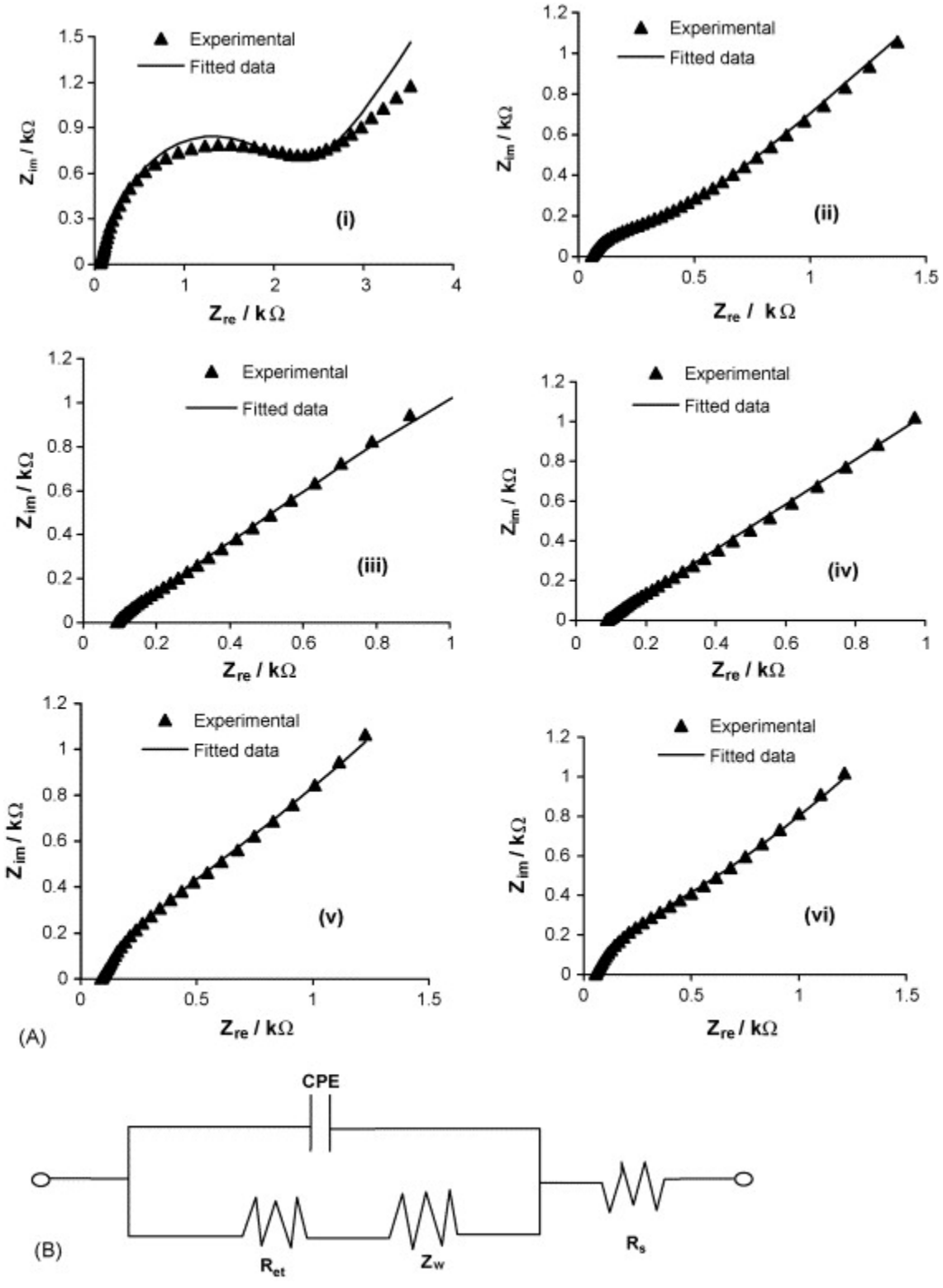

Fig. 4. (A) Nyquist plots resulting from (i) bare BPPGE, (ii) BPPGE-CoTAPc, (iii) BPPGE-SWCNT, (iv) BPPGE-SWCNT-CoTAPc$_{(mix)}$, (v) BPPGE-SWCNT-CoTAPc$_{(cov)}$

and (vi) BPPGE-SWCNT-CoTAPc$_{(ads)}$ in 0.1 M KCl containing equimolar mixture of $K_4Fe(CN)_6$ and $K_3Fe(CN)_6$. (B) Simple equivalent circuit model.

Given the inherent roughness of the BPPGE, the constant phase angle element (CPE), in which the double layer capacitance is replaced by CPE in the Randles' model [43] was used to explain the EIS data obtained in this work. The impedance data were fitted to an equivalent circuit using the FRA software package for complex non-linear least squares (NNLS) calculations based on the EQUIVCRT programme. As shown in the Nyquist plots, the simple equivalent circuit model showed good agreement with the experimental results. Table 2 summarises the obtained parameters for the equivalent circuit model.

Table 2.

Summary of estimated EIS parameters obtained for the electrodes (errors ≤0.3%)

Electrodes	R_s **(Ω)**	R_{et} **(kΩ)**	**CPE (μF)**	Z_w **(Ω s$^{-1/2}$)**	***n***	k_{app} **(cm s^{-1})**
Bare BPPGE	64.30	2.16	0.68	6.35×10^{-4}	0.80	2.42×10^{-5}
BPPGE-CoTAPc	53.80	0.41	1.48	7.95×10^{-4}	0.69	12.90×10^{-5}
BPPGE-SWCNT	90.71	0.27	0.19	6.50×10^{-4}	0.73	19.22×10^{-5}
BPPGE-SWCNT-CoTAPc$_{(mix)}$	89.12	0.22	14.81	7.37×10^{-4}	0.72	23.6×10^{-5}
BPPGE-SWCNT-CoTAPc$_{(cov)}$	88.03	1.12	15.13	7.99×10^{-4}	0.71	4.68×10^{-5}
BPPGE-SWCNT-CoTAPc$_{(ads)}$	53.74	0.61	21.01	8.77×10^{-4}	0.77	8.35×10^{-5}

The Z_w values, which correspond to the diffusion process of the oxidised and reduced species of the $[Fe(CN)_6]^{3-/4-}$ couple, are approximately of the same magnitude for all the electrodes. Ideally, R_s and Z_w should not be affected by modification of the electrode surface [45]. The increase in R_s (~40%) observed in BPPGE-SWCNT, BPPGE-SWCNT-CoTAPc$_{(cov)}$ and BPPGE-SWCNT-CoTAPc$_{(mix)}$ is not fully understood at this time but may be related to the resistances induced by these films. The possible explanation for the apparent increase in the Z_w values of other electrodes compared to that of the BPPGE is that the modifiers (CoTAPc, SWCNT or SWCNT-CoTAPc) act as individual particles on the BPPGE surface making the $[Fe(CN)_6]^{3-/4-}$ redox species more difficult to diffuse to

the electrode BPPGE surface, thereby increasing the Warburg impedance. The relatively higher CPE value for BPPGE-SWCNT-CoTAPc$_{(ads)}$ indicates that this type of electrodeposition offers a more uniform or homogenous film compared to the drop-dry method. The *n*-values (<1.0) indicate that the electrodes are not true capacitors. The apparent electron transfer rate constant k_{app} was obtained from the following equation [46]:

$$k_{app} = \frac{RT}{F^2 R_{et} C} \quad (8)$$

where R is the gas constant (8.314 J mol^{-1} K^{-1}), T the absolute temperature of the system (298 K), F the Faraday constant (96,485 C mol^{-1}), and C is the concentration of the $[Fe(CN)_6]^{3-}$ (in mol cm^{-3}, the concentration of $[Fe(CN)_6]^{3-}$ and $[Fe(CN)_6]^{4-}$ are equal). From Table 1, we observed a significant decrease in the R_{et} values for the modified electrodes compared to that of the bare BPPGE which confirm that the charge transfer processes on the modified electrodes for $[Fe(CN)_6]^{3-/4-}$ are easier than in the bare BPPGE. From the Bode plots of phase angle versus log f (Fig. 5a), it is seen that the bare BPPGE showed well-defined symmetrical peak with a maximum value of ~54° at 158 Hz corresponding to the relaxation process of the BPPGE|solution interface. On modification of the BPPGE, this relaxation process shifts to different phase angles (*ca*. 34–42° range) and at lower frequencies (1.4–6.4 Hz range). These shifts indicate that the reactions now occur at the surface of the modifying films rather than the bare BPPGE.

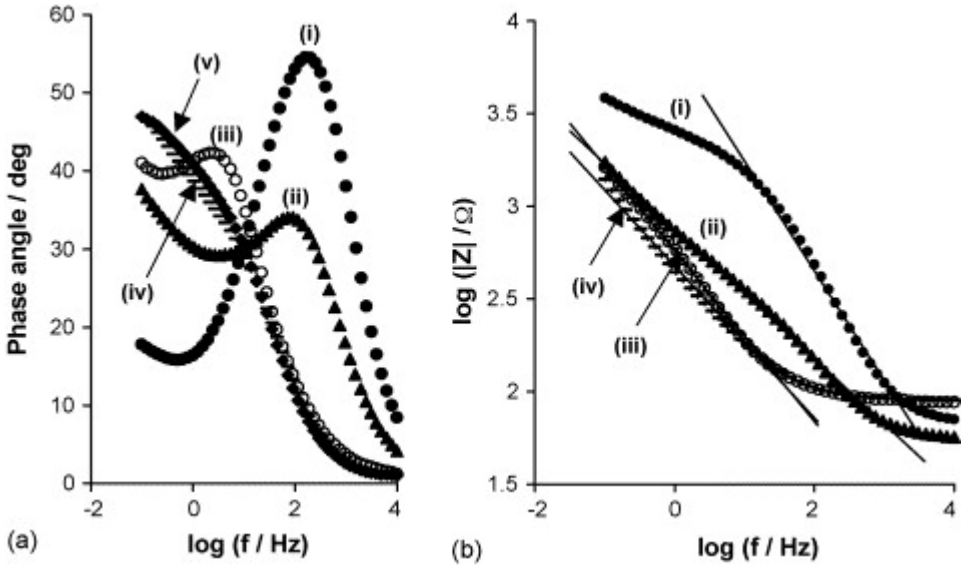

Fig. 5. Bode plots of (a) phase angle vs. logarithm of frequency and (b) logarithm of complex impedance vs. logarithm of frequency for the (i) bare BPPGE, (ii) BPPGE-CoTAPc, (iii) BPPGE-SWCNT-$CoPc_{(cov)}$, (iv) BPPGE-SWCNT-$CoTAPc_{(mix)}$ and (v) BPPGE-SWCNT in 0.1 M KCl containing equimolar mixture of $K_4Fe(CN)_6$ and $K_3Fe(CN)_6$. BPPGE-SWCNT and BPPGE-SWCNT-$CoTAPc_{(ads)}$ showed similar spectra as the BPPGE-SWCNT-$CoTAPc_{(mix}$ and BPPGE-SWCNT-$CoTAPc_{(cov)}$ and so have been omitted for clarity.

The Bode plots (log|Z| versus log *f*) (Fig. 5b) gave the following slopes; −0.593 (r^2 = 0.993), −0.351 (r^2 = 0.998), −0.459 (r^2 = 0.998), −0.410 (r^2 = 0.993) and −0.410 (r^2 = 0.993) for BPPGE, BPPGE-CoTAPc, BPPGE-SWCNT-$CoTAPc_{(cov)}$, BPPGE-SWCNT-$CoTAPc_{(mix)}$ and BPPGE-SWCNT, respectively. The slopes are far away from the ideal −1.0 value, further corroborating the CPE data in Table 2 that these electrodes are not true capacitors. As reflected in their k_{app} and R_{et} values, BPPGE-SWCNT and BPPGE-SWCNT-$CoTAPc_{(mix)}$ exhibited faster electron transfer processes towards $[Fe(CN)_6]^{3-/4-}$ compared to other electrodes investigated in this work. Thus, all subsequent studies, unless otherwise stated, were carried out with these two electrodes.

3.3. Electrocatalysis of V-type nerve agents degradation products

3.3.1. Effect of pH changes

BPPGE-SWCNT-CoTAPc$_{(mix)}$ was used to ascertain the effect of different solution pHs on the catalytic detections of the DEAET and DMAET. Fig. 6 shows an example of the cyclic voltammetric responses (i.e., peak potential and peak currents) obtained for DEAET (10^{-4} M) at different solution pHs (2.0–12.0). Similar voltammetric profiles were obtained for DMAET at the same pH range.

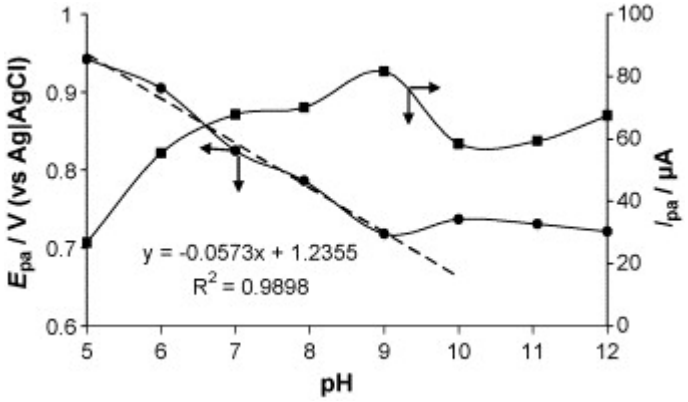

Fig. 6. Plots of E_{pa} and I_{pa} vs. pH for DEAET (10^{-4} M) using BPPGE-SWCNT-CoTAPc$_{(mix)}$. Arrow directions indicate the respective axes for each of the plots. The broken line is the straight line plot for the E_{pa} vs. pH (pH 5–9) extracted from the E_{pa} vs. pH (pH 5–12) curve. Scan rate, 50 mV s^{-1}.

For both analytes, no detectable catalytic current was observed at pH ≤ 5.0. However, in the pH 5.0–9.0 range, we obtained linear plots of E_p versus pH with slopes of −57 mV/pH, indicating approximately equal electron and proton transfer process. Maximum catalytic currents were observed at equal or greater than pH 9.0 for both analytes. This behaviour is consistent with the pK_a of DEAET reported as 8.3 at 25 °C [47]. Thus, all subsequent studies here for DMAET, DEAET were performed at pH 9.3 PBS with some works at physiological pH 7.4 conditions.

3.3.2. Comparative catalytic responses of different electrodes

Fig. 7 shows typical CVs obtained at different electrodes for the electrocatalytic detection of DMAET.

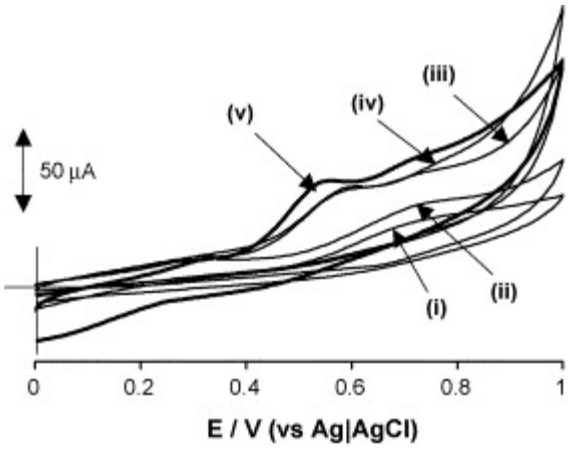

Fig. 7. Typical comparative cyclic voltammograms for 10^{-4} M DMAET in pH 9.3 PBS at different electrodes: (i) bare BPPGE, (ii) BPPGE-CoTAPc, (iii) BPPGE-SWCNT-CoTAPc$_{(mix)}$, (iv) BPPGE-SWCNT-CoTAPc$_{(syn)}$ and (v) BPPGE-SWCNT. All electrodes were obtained by drop-dry method. Scan rate, 50 mV s^{-1}.

As seen in Fig. 7, BPPGE-SWCNT gave slightly higher catalytic current at less potential (with higher background current) when compared to other electrodes. Similar experiment with DEAET, using the same concentration as for DMAET, gave slightly higher (~10%) catalytic current response at less potential. In summary, the background-corrected catalytic current responses for both analytes follow this trend: BPPGE-SWCNT ≈ BPPGE-SWCNT-CoTAPc$_{(mix)}$ ≈ BPPGE-SWCNT-CoTAPc$_{(cov)}$ ≈ BPPGE-SWCNT-CoTAPc$_{(ads)}$ > BPPGE-CoTAPc > Bare BPPGE. Given its relatively higher sensitivity over cyclic voltammetry, SWV was used to probe the response of the two electrodes, BPPGE-SWCNT and BPPGE-SWCNT-CoTAPc$_{(mix)}$ towards the detection of DMAET and DEAET. As clearly evident in Fig. 8, SWCNT-CoTAPc$_{(mix)}$ film showed better potential discrimination for the two sulfhydryls than with the SWCNT film; while both analytes can be detected at the same potential (*ca*. 0.55 V versus Ag|AgCl) at the BPPGE-SWCNT, the BPPGE-SWCNT-CoTAPc$_{(mix)}$ make them appear at different potentials (*ca*. 0.64 and 0.73 V versus Ag|AgCl for DEAET and DMAET, respectively).

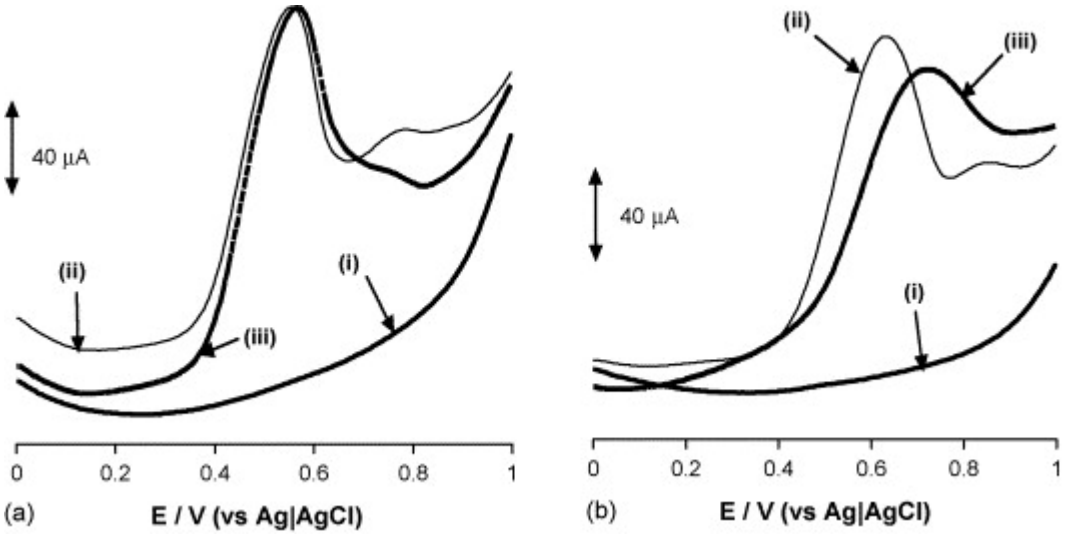

Fig. 8. Square wave voltammetric profiles for (a) BPPGE-SWCNT and (b) BPPGE-SWCNT-CoTAPc$_{(mix)}$ in (i) buffer, (ii) DEAET, and (iii) DMAET in pH 9.3 buffer solution. Concentration of individual analyte and when mixed were maintained at 10^{-4} M.

Remarkable results observed herein are worthy of note. First, the double oxidation peaks seen at the electrodes (most pronounced at the BPPGE-SWCNT than other electrodes, Fig. 7 and Fig. 8) are typical of CNT-based electrodes for thiols and related analytes [23] and [35]. Based on such reports, we ascribe the first oxidation peak (example in Fig. 8a at 0.55 V) to be mediated by the quinone-like functional groups at the tube ends of the SWCNT (artefact of acid purification), while the second oxidation peak (as in Fig. 8a at ~0.73 V) to be mediated by the edge plane-like carbon at the SWCNT. Second, CoTAPc activity is enhanced by the presence of SWCNT, and SWCNT-COTAPc improves the greatly the electronic communication between DMAET or DEAET and the BPPGE. The enhanced electrocatalytic activity in the presence of SWCNT is not surprising as electrodes modified with SWCNT have been known to exhibit better catalytic activity compared to their unmodified electrodes [36]. It should be mentioned here that a preliminary EDX experiment reveals the presence of nickel impurities in the SWCNTs used in this work. Such metal impurities may affect the catalysis of SWCNT, as reported recently by Compton and co-workers for MWCNTs [48], however, this will be the focus of future investigations for our SWCNT-modified electrodes. Third, it is interesting to note that the three SWCNT-CoTAPc based electrodes gave similar current responses

towards the catalytic detection of these V-type nerve agents, suggesting that the long synthetic processes for the SWCNT-CoTAPc$_{(cov)}$ can be avoided for this type of work. Thus, all subsequent electrocatalysis experiments for these thiols were performed with the BPPGE-SWCNT-CoTAPc$_{(mix)}$.

A plot of peak current (I_p) against the square root of scan rate ($v^{1/2}$) resulted in a straight line, which is an indication that the electrocatalytic oxidation of DMAET and DEAET are diffusion controlled reactions. However, at higher scan rates (300–1200 mV s^{-1}) the I_p versus $v^{1/2}$ plot became non-linear, most likely due to the adsorption of these sulfhydryls on the surface of the electrodes. Secondly, a plot of $I_{pa}/v^{1/2}$ against v (not shown) resulted in the characteristic shape that is typical for catalytic process of electrochemical reaction preceding chemical reaction (EC_{cat}) processes [49]. A plot of E_p versus (1/2)log v (not shown), used for an irreversible, diffusion controlled processes [50], [51] and [52], gave Tafel slope ($b = 2.303RT/\alpha nF$) of approximately 219 and 243 mV $decade^{-1}$ for DEAET and DMAET, respectively. Assuming an electrochemical transfer coefficient (α) <0.5, these results indicate that the rate-determining step for the catalysis of these sulfhydryls involve one-electron transfer process. It is well established [53], [54] and [55] that high Tafel slopes ($\alpha < 0.5$) as obtained in this study is the consequence of strong binding of reactants or intermediates on the electrode surfaces and/or reactions occurring within a porous electrode structure. Thus, we associate the doubled Tafel slopes obtained in this work to the strong binding of these sulfhydryls with the SWCNT-CoTAPc catalyst.

Repetitive scanning experiments with these sulfhydryls at constant concentration showed electrode poisoning. However, on rinsing the fouled electrode by 5 repetitive-scanning in buffer solution alone, ~90% recovery was observed. This electrode fouling also agrees with binding of the analytes with the SWCNT-CoTAPc.

Mechanisms for the electrocatalytic oxidation of sulfhydryls using MPc-based electrodes are widely reported [23], [56], [57] and [58]. We believe that similar mechanism could well apply to these two related sulfhydryl species, as shown below:

$$RSH + OH^- \rightarrow RS^- + H_2O \qquad (9)$$

$$RS^- + Co(II)TAPc \rightarrow [(SR)–Co(III)TAPc]^- \quad (10)$$

$$[(SR)–Co(III)TAPc]^- \rightarrow [(SR)–Co(III)TAPc] + e^- \text{ (rds)} \quad (11)$$

$$[(SR)–Co(III)TAPc] \rightarrow Co(II)TAPc + RS\cdot \quad (12)$$

$$2RS\cdot \rightarrow RSSR \text{ (fast)} \quad (13)$$

RSH denotes the sulfhydryl nerve-agent hydrolysis products (DMAET and DEAET), RS**.** is thiyl radical, while RSSR is the disulphide products. Eq. (9) is known for DEAET in basic solution [47]. Eq. (11) is related to the rate-determining step (rds) as discussed in Tafel slope. In general, the process involves an initial oxidation of the Co(II)TAPc to Co(III)TAPc followed by the generation of the thiyl radical via Co(III)TAPc and subsequent regeneration of the Co(II)TAPc species.

3.3.3. Chronoamperometric analysis

Based on the SWV results described above, chronoamperometric technique was employed for the analysis of these two analytes in pH 9.3 PBS at different potentials (+640 and 730 mV versus Ag|AgCl for DEAET and DMAET, respectively) using BPPGE-SWCNT-CoTAPc$_{(mix)}$. From the current responses of the BPPGE-SWCNT-CoTAPc$_{(mix)}$ to changes in the concentrations of these sulfhydryls, we found that they could be detected down to approximately 8.0 μM for DMAET and 3.0 μM for DEAET with good sensitivities (≈5.0 and 6.0 × 10^{-2} A M^{-1} for DMAET and DEAET, respectively).

Also, using the BPPGE-SWCNT-CoTAPc$_{(mix)}$, we determined the catalytic rate constants and diffusion coefficients of these analytes at constant concentration (at 10^{-3} M in pH 9.3 PBS) poised at +640 and 730 mV versus Ag|AgCl for DEAET and DMAET, respectively. At intermediate times (0.5–2.2 s) of the chronoamperometric measurements, the catalytic currents (I_{cat}) were dominated by the rate of the electrocatalysed oxidation of these nerve agents, thus the rate constants for the chemical reactions between the nerve

agents and redox sites of surface-immobilised SWCNT-CoTAPc$_{(mix)}$ were determined using the established equation [59], [60] and [61]:

$$\frac{I_{cat}}{I_L} = \pi^{1/2}(kC_0t)^{1/2} \quad (14)$$

where I_{cat} and I_L are the currents of the BPPGE-SWCNT-CoTAPc$_{(mix)}$ in the presence and absence of the analytes, respectively, and C_0 is the bulk concentration of analytes, k and t are the catalytic rate constant (M^{-1} s^{-1}) and time elapsed (s). From the slopes of the plots of I_{cat}/I_L versus $t^{1/2}$ (1.1845 and 1.8784 $s^{-1/2}$ for DMAET and DEAET, respectively) and at the concentration of 10^{-3} M for these sulfhydryls, the values of k were found to be 1123.59 M^{-1} s^{-1} for DEAET and 893.67 M^{-1} s^{-1} for DMAET. This shows that the electrocatalytic oxidation of these analytes is fast at SWCNT-CoTAPc films. Also, employing the Cottrell equation:

$$I=nFD^{1/2}AC_0\pi^{-1/2}t^{-1/2} \quad (15)$$

the diffusion coefficient, D, for DMAET and DEAET were determined from the slopes of plots of I versus $t^{-1/2}$ to be approximately 2.30×10^{-5} and 1.50×10^{-5} cm^2 s^{-1} for DEAET and DMAET, respectively. At this juncture, it is important to note that there are no accessible literature at the moment to compare our electrocatalytic parameters obtained here for these two thiol-degradation products, the few known reports [62] and [63] only dealt with their amperometric detection. Thus, this work is the first to provide detailed electrocatalytic parameters for DEAET and DMAET.

4. Conclusion

We have shown in this work detailed electrochemical and electrocatalytic behaviour of single-wall carbon nanotube (SWCNT) and SWCNT functionalised with cobalt (II) tetra-aminophthalocyanine. It is proved amongst others that SWCNT clearly enhances both the solution and surface electrochemistry of CoTAPc. The study is unique in that it provides for the first time the electrocatalytic parameters for the sulfhydryl hydrolysis products of V-type agents. BPPGE-SWCNT-CoTAPc$_{(mix)}$ and BPPGE-SWCNT showed comparable electrocatalytic responses towards the detection of V-type nerve agent sulfhydryl

hydrolysis products, BPPGE-SWCNT-CoTAPc showed better potential discrimination for the detection of these sulfhydryl analytes than the BPPGE-SWCNT. It is possible that this type of electrode modification with SWCNT could provide the means for controlled fabrication of sensitive electrochemical sensors based on many other transition metal phthalocyanine and porphyrin complexes substituted with amino-functionality. This possibility is currently being explored in our laboratory.

References

[1] Q. Yan, G. Zhou, S. Hao, J. Wu and W. Duan, *Appl. Phys. Lett.* **88** (2006), p. 173107/1.

[2] W.B. Choi, E. Bae, D. Kang, S. Chae, B.-H. Cheong, J.-H. Ko, E. Lee and W. Park, *Nanotechnology* **15** (2004), p. S512.

[3] K. Tsukagoshi, N. Yoneya, S. Uryu, Y. Aoyagi, A. Kanda, Y. Ootuka and B.W. Alphenaar, *Phys. B: Condens. Matter* **323** (2002), p. 107.

[4] J.A. Rojas-Chapana and M.J. Giersig, *J. Nanosci. Nanotechnol.* **6** (2006), p. 316.

[5] S.K. Smart, A.I. Cassady, G.Q. Lu and D.J. Martin, *Carbon* **44** (2006), p. 1034.

[6] A. Bianco, K. Kostarelos and M. Prato, *Curr. Opin. Chem. Biol.* **9** (2005), p. 674.

[7] M. Musameh, J. Wang, A. Merkoki and Y. Lin, *Electrochem. Commun.* **4** (2002), p. 743.

[8] C.E. Banks, R.R. Moore, T.J. Davies and R.G. Compton, *Chem. Commun.* (2004), p. 1804.

[9] K. Gong, Y. Yan, M. Zhang, L. Su, S. Xiong and L. Mao, *Anal. Sci.* **21** (2005), p. 1383.

[10] A. Merkoci, M. Pumera, X. Llopis, B. Perez, M. del Valle and S. Alegret, *TrAC* **24** (2005), p. 826. |

[11] J.J. Gooding, *Electrochim. Acta* **50** (2005), p. 3049.

[12] Y.-H. Yun, V. Shanov, M.J. Schulz, S. Narasimhadevara, S. Subramaniam, D. Hurd and F.J. Boerio, *Smart Mater. Struct.* **14** (2005), p. 1526.

[13] T. Hasobe, S. Fukuzumi and P.V. Kamat, *J. Am. Chem. Soc.* **127** (2005), p. 11884.

[14] R.J. Chen, Y. Zhang, D. Wang and H. Dai, *J. Am. Chem. Soc.* **123** (2001), p. 3838.

[15] Z.-L. Yang, H.-Z. Chen, L. Cao, H.-Y. Li and M. Wang, *Mater. Sci. Eng.* **B106** (2004), p. 73.
[16] G. de la Torre, W. Blau and T. Torres, *Nanotechnology* **14** (2003), p. 765.
[17] K.I. Ozoemena and T. Nyokong In: C.A. Grimes, E.C. Dickey and M.V. Pishko, Editors, *Encyclopedia of Sensors* **vol. 3**, American Scientific Publishers, California (2006), p. 157 (Chapter E, and references therein).
[18] X. Wang, Y. Liu, W. Qiu and D. Zhu, *J. Mater. Chem.* **12** (2002), p. 1636.
[19] A. Salimi, C.E. Banks and R.G. Compton, *Analyst* **129** (2004), p. 225.
[20] C.E. Banks, R.R. Moore, T.J. Davies and R.G. Compton, *Chem. Commun.* **16** (2004), p. 1804.
[21] R.R. Moore, C.E. Banks and R.G. Compton, *Anal. Chem.* **76** (2004), p. 2677.
[22] G.G. Wildgoose, H.G. Leventis, I. Streeter, N.S. Lawrence, S.J. Wilkins, L. Jiang, T.G.J. Jones and R.G. Compton, *ChemPhysChem* **5** (2004), p. 669.
[23] M.P. Siswana, K.I. Ozoemena and T. Nyokong, *Electrochim. Acta* **52** (2006), p. 114.
[24] K.I. Ozoemena, J. Pillay and T. Nyokong, *Electrochem. Commun.* **8** (2006), p. 1391.
[25] E.W. Hooijschuur, A. Hulst, A. de Long, L. de Reuver, S. van Krimpen, B. van Baar, E. Wils, C. Kientz and U.A. Brinkman, *Trends Anal. Chem.* **21** (2002), p. 116.
[26] Y. Yang, *Acc. Chem. Res.* **32** (1999), p. 109.
[27] B.N. Achar, G.M. Fohlen and J.A. Parker, *J. Polym. Sci.* **20** (1982), p. 2773.
[28] S.W. Oliver and T.D. Thomas, *Heterocycles* **22** (1984), p. 2047.
[29] B.N. Achar, G.M. Fohlen, J.A. Parker and J. Keshavaya, *Polyhedron* **6** (1987), p. 1463.
[30] J. Liu, A.G. Rinzler, H. Dai, J.H. Hanfer, R.K. Bradley, P.J. Boul, A. Lu, T. Iverson, K. Shelimov, C.B. Huffman, F.R. Macias, Y.S. Shon, T.R. Lee, D.T. Colbert and R.E. Smalley, *Science* **280** (1998), p. 1253.
[31] J. Chen, M.A. Hamon, H. Hu, Y. Chen, A.M. Rao, P.C. Eklund and R.C. Haddon, *Science* **282** (1998), p. 95.
[32] B.A. Boukamp, *Solid State Ionics* **20** (1986), p. 31.
[33] A.B.P. Lever, E.R. Milaeva and G. Speier In: A.P.B. Lever and C.C. Leznoff, Editors, *Phthalocyanines: Properties and Applications* **vol. 3**, VCH Publishers, New York (1993).

[34] X.-Y. Xiao and S.-G. Sun, *Electrochim. Acta* **45** (2000), p. 2897.

[35] W. Yang, J.J. Gooding and D.B. Hibbert, *J. Electroanal. Chem.* **516** (2001), p. 10.

[36] K. Gong, X. Zhu, R. Zhao, S. Xiong, L. Mao and C. Cheng, *Anal. Chem.* **77** (2005), p. 8158.

[37] C. Hu, X. Cheng and S. Hu, *J. Electroanal. Chem.* **586** (2006), p. 77.

[38] J. Wang, Analytical Electrochemistry, VCH Publishers, New York (1994).

[39] E. Laviron, *J. Electroanal. Chem.* **52** (1974), p. 355.

[40] E. Laviron, *J. Electroanal. Chem.* **101** (1979), p. 19.

[41] K.I. Ozoemena and T. Nyokong, *Electrochim. Acta* **51** (2006), p. 2669.

[42] E. Katz and I. Wilner In: V.M. Mirsky, Editor, *Ultrathin Electrochemical Chemo- and Biosensors. Technology and Performance*, Springer-Verlag, New York (2004), p. 68 (Chapter 4).

[43] D.D. MacDonald, *Electrochim. Acta* **51** (2006), p. 1376.

[44] S. Griveau, J. Pavez, J.H. Zagal and F. Bedoui, *J. Electroanal. Chem.* **497** (2001), p. 75.

[45] L. Yang and Y. Li, *Biosens. Bioelectron.* **20** (2005), p. 1407.

[46] E. Sabatini and I. Rubinstein, *J. Phys. Chem.* **91** (1987), p. 6663.

[47] Y.-C. Yang, L.L. Szafraniec, W.T. Beaudry, D.K. Rohrbaugh, L.R. Procell and J.B. Samuel, *J. Org. Chem.* **61** (1996), p. 8407.

[48] C.E. Banks, A. Crossley, C. Salter, S.J. Wilkins and R.G. Compton, *Angew. Chem. Intl. Ed.* **45** (2006), p. 2533.

[49] S.M. Golabi and H.R. Zare, *J. Electroanal. Chem.* **465** (1999), p. 168.

[50] J. Zhang, Y.-H. Tse, W.J. Pietro and A.B.P. Lever, *J. Electroanal. Chem.* **406** (1996), p. 203.

[51] J.H. Zagal and M.A. Paez, *Electrochim. Acta* **42** (1997), p. 3477.

[52] L. Niu, T. You, J.Y. Gui, E. Wang and S. Dong, *J. Electroanal. Chem.* **448** (1998), p. 79.

[53] B. Wermeckers and F. Beck, *Electrochim. Acta* **30** (1985), p. 1491.

[54] J.-M. Zen, A.S. Kumar and M.-R. Chang, *Electrochim. Acta* **45** (2000), p. 1691.

[55] J.N. Soderberg, A.C. Co, A.H.C. Sirk and V.I. Birss, *J. Phys. Chem. B* **110** (2006), p. 10401.

[56] M.K. Halbert and R.P. Baldwin, *Anal. Chem.* **57** (1985), p. 591.

[57] S. Maree and T. Nyokong, *J. Electroanal. Chem.* **492** (2000), p. 120.

[58] N. Sehlotho and T. Nyokong, *Electrochim. Acta* **51** (2006), p. 4463.

[59] M.H. Pournaghi-Azar and R. Sabzi, *J. Electroanal. Chem.* **543** (2003), p. 115.

[60] P. Santhosh, K.M. Manesh, K.-P. Lee and A.I. Gopalan, *Electroanalysis* **18** (2006), p. 894.

[61] K.M. Manesh, P. Santhosh, A.I. Gopalan and K.-P. Lee, *Electroanalysis* **18** (2006), p. 1564.

[62] J. Wang, J. Zima, N.S. Lawrence and M.P. Chatrathi, *Anal. Chem.* **76** (2004), p. 4721.

[63] K.A. Joshi, M. Prouza, M. Kum, J. Wang, J. Tang, R. Haddon, W. Chen and A. Mulchandani, *Anal. Chem.* **78** (2006), p. 331.